Published online March 8, 2006

Root Zone Soil Moisture Assessment Using Remote Sensing and Vadose Zone Modeling

Narendra N. Das and Binayak P. Mohanty*

ABSTRACT

Soil moisture is an important hydrologic state variable critical to successful hydroclimatic and environmental predictions. Soil moisture varies both in space and time because of spatio-temporal variations in precipitation, soil properties, topographic features, and vegetation characteristics. In recent years, air- and space-borne remote sensing campaigns have successfully demonstrated the use of passive microwave remote sensing to map soil moisture status near the soil surface (≈0–0.05 m below the ground) at various spatial scales. In this study root zone (e.g., ≈0–0.6 m below the ground) soil moisture distributions were estimated across the Little Washita watershed (Oklahoma) by assimilating near-surface soil moisture data from remote sensing measurements using the Electronically Scanned Thinned Array Radiometer (ESTAR) with an ensemble Kalman filter (EnKF) technique coupled with a numerical one-dimensional vadose zone flow model (HYDRUS-ET). The resulting distributed root zone soil moisture assessment tool (SMAT) is based on the concept of having parallel noninteracting streamtubes (hydrologic units) within a geographic information system (GIS) platform. The simulated soil moisture distribution at various depths and locations within the watershed were compared with measured profile soil moisture data using time domain reflectometry (TDR). A reasonable agreement was found under favorable conditions between footprint-scale model estimations and point-scale field soil moisture measurements in the root zone. However, uncertainties introduced by precipitation and soil hydraulic properties caused suboptimal performance of the integrated model. The SMAT holds great promise and offers flexibility to incorporate various data assimilation techniques, scaling, and other hydrological complexities across large landscapes. The integrated model can be useful for simulating profile soil moisture estimation and for predicting transient soil moisture behavior for a range of hydrological and environmental applications.

Spatio-temporal distributions of soil moisture status in the root zone across large land areas provide important input for many agricultural, hydrological, and meteorological applications (Hanson et al., 1999). Also, estimation of root zone soil moisture at various temporal and spatial scales is key to strategic management of water resources. Root zone soil moisture is a critical storage parameter, which controls partitioning of energy and mass related to evapotranspiration and runoff (Georgakakos, 1996). Precipitation, soil texture, topography, land use, and a variety of meteorological variables influence the spatial distribution and temporal evolution of root zone soil moisture. Many studies at the Southern Great Plains 1997 Hydrology Experiment (SGP97) site have examined how these variables influence the spatiotemporal distribution of soil moisture and surface fluxes (Famiglietti et al., 1999; Mohr et al., 2000; Mohanty et al., 2000a, 2000b; Mohanty and Skaggs, 2001; Bindlish et al., 2001; Kustas et al., 2001; Wickel et al., 2001). The estimation of soil moisture and energy–mass exchange is simulated using soil–vegetation–atmosphere transfer models (SVAT). The accuracy of SVAT models is usually restricted by unreliable estimates of root zone soil moisture (Koster and Milly, 1997). Despite the significance of root zone soil moisture in hydrological and meteorological predictions, detailed spatiotemporal modeling of root zone soil moisture at the regional or global scale is often lacking.

Root zone soil moisture distributions are best assessed by periodic gravimetric sampling or by calibrated TDR techniques. At a particular location, soil moisture can be continuously monitored by calibrating segmented TDR probes (e.g., Hook and Livingston, 1996) or by multisensor capacitance probes (e.g., Starr and Paltineanu, 1998). Camillo and Schmugge (1983) retrieved root zone soil moisture estimates from surface measurement for dry soil with fully grown roots using a linear relationship between moisture content in the two soil layers based on a simple solution of Richards' equation. These techniques serve well for field plot or local-scale monitoring but are not feasible for the watershed or regional scale. Remote sensing of soil moisture from air- or space-borne platforms has the ability to overcome this problem and provide large spatial coverage and temporal continuity. In the last three decades studies have successfully established the use of passive microwave remote sensing to measure the surface wetness (Engman and Gurney, 1991; Jackson, 1993; Njoku and Entekhabi, 1995; Jackson et al., 1999). These measurements described soil moisture in a thin soil layer, usually up to a depth of 0.05 m below the soil surface (Schmugge et al., 1974, 1977, 1980; Jackson and Schmugge, 1989). However, an associated problem that has hindered the measurement of soil moisture from air and space using passive microwave techniques is its coarse spatial and temporal resolution, which is not consistent with the scale of hydrologic processes of interest.

Prevot et al. (1984) demonstrated that the soil water balance could be determined with equal accuracy using remotely sensed surface soil moisture estimates substituted for in situ observations. Smith and Newton (1983) developed a soil water simulation model that used remotely sensed data to predict profile soil moisture. In

N.N. Das and B.P. Mohanty, Department of Biological and Agricultural Engineering, Texas A&M University, College Station, TX 77843-2117. Received 6 Mar. 2005. *Corresponding author (bmohanty@tamu.edu).

Published in Vadose Zone Journal 5:296–307 (2006).
Special Section: From Field- to Landscape-Scale Vadose Zone Processes
doi:10.2136/vzj2005.0033

677 S. Segoe Rd., Madison, WI 53711 USA

Abbreviations: DOY, day of year; EnKF, ensemble Kalman filter; ESTAR, Electronically Scanned Thinned Array Radiometer; GIS, geographic information system; LULC, land use land cover; LW, Little Washita; SGP97, Southern Great Plains 1997 Hydrology experiment; SMAT, soil moisture assessment tool; SVAT, soil–vegetation–atmosphere transfer; TDR, time domain reflectometry.

the recent past, studies have been conducted on improving assessment of profile soil moisture with the help of surface soil moisture observations (Kostov and Jackson, 1993; Entekhabi et al., 1994). Jackson (1993) elaborated four strategies using surface soil moisture data to estimate profile soil moisture: (i) statistical extrapolation of the surface observation, (ii) integration of surface observations in a profile water budget model, (iii) inversion of radiative transfer model, and (iv) the parametric profile model method. Kostov and Jackson (1993) presented a detailed review of these basic approaches for estimating profile soil moisture using remotely sensed surface moisture data and concluded that the most promising approach to the problem of profile soil moisture estimation was the integration of remote sensing and computational modeling. An illustration of this concept has been provided by Entekhabi et al. (1994) in their theoretical approach for solving the inverse problem for soil moisture using sequential assimilation of remotely sensed surface data. Houser et al. (1998) studied the use of four-dimensional data assimilation methods in a macroscale land hydrology model to generate root zone moisture fields on regular space and time intervals. Several other studies were conducted using data from the Southern Great Plains 1997 (SGP97) hydrology experiment (Jackson et al., 1999), and the concepts were tested at the point scale (Crosson et al., 2002; Starks et al., 2003; Heathman et al., 2003; Crow and Wood, 2003). Walker et al. (2001) explored the effects of observation depth and update interval on soil moisture profile retrieval and made a comparison of two commonly used assimilation techniques (i.e., direct insertion and Kalman filter) using synthetic data. They concluded that Kalman filter assimilation scheme is superior to the direct insertion assimilation scheme. Profile retrieval was unsuccessful for direct insertion using the surface node alone; observations over some nonzero depth were required. The superiority of the Kalman filter lies in its ability to adjust the entire profile, while direct insertion can only alter the profile within the observation depth. On the contrary, Heathman et al. (2003) investigated profile soil water content using direct data assimilation in the root zone water quality model at four field sites in the Little Washita (LW) River Experimental Watershed during SGP97, and found that direct insertion assimilation improved model estimates down to a depth of 0.30 m at all the sites considered in their study, and no significant improvement in soil water estimates below the 0.30-m depth. Crosson et al. (2002) applied the Kalman Filter based method for assimilating remotely sensed (ESTAR-based, during SGP97) soil moisture estimates in a point-scale testing scheme and found that even in the presence of highly inaccurate rainfall the model results in good agreement with observed soil moisture. Crow and Wood (2003) extended EnKF methodology to assimilate remotely sensed (ESTAR, SGP97) soil moisture data into a land surface model and validated against independent observations. They found that root zone soil moisture predictions made with the EnKF are more accurate than predictions derived from direct assimilation of ESTAR surface soil moisture imagery. Recently, Dunne and Entekhabi (2005) used ESTAR pixel and field data of SGP97 to investigate an ensemble-based reanalysis (ensemble-based smoother) approach to land data assimilation. They demonstrated that smoothing improved the estimated soil moisture at the soil surface and at deeper depths over EnKF estimation. The performance of EnKF was also studied by Reichle et al. (2002) and Margulis et al. (2002), where soil moisture estimation is assessed by assimilating L-band (1.4 GHz) microwave observations into a land surface model. They showed that EnKF is a flexible and robust data assimilation technique that gives satisfactory estimates even for moderate ensemble size. From these, it is clear that EnKF offers several advantages over traditional methods of data assimilation for retrieving soil moisture from microwave remote sensing.

Generally, data assimilation is used in conjunction with a SVAT (land surface model, LSM) model. The model can be treated as a stand-alone program, which communicates with the filter through its input and output files. The filter provides a set of random initial conditions, parameters, and forcing variables to the land surface model. In turn, the model derives a time-dependent state vector that is passed to the filtering algorithm. This modularity makes it possible to use nearly any land surface model in a data assimilation procedure based on an EnKF. The most frequently used SVAT models with data assimilation are the NOAH model (Chen et al., 1996), Variable Infiltration Capacity (VIC) model (Liang et al., 1996), Mosaic model (Koster and Suarez, 1996), and Common Land Model (CLM; Dai et al., 2003). The SVAT models typically include a thin surface soil layer and one or more thicker root zone layers and estimate soil moisture of each soil layer at the land–atmosphere boundary and the interfaces between the soil layers. The SVAT models run typically in an uncoupled fashion using a number of generic tools to manage the input and output data. From the vadose zone hydrology perspective at the landscape scale or larger, there is a need for simple and robust integration of surface remote sensing information into a dynamic soil water model in a distributed computing platform (e.g., GIS) to improve the simulation of root zone soil moisture.

For distributed models, GIS is considered the best available tool for organizing and processing data at the watershed/regional scale (Thieken et al., 1999; Lachassagne et al., 2001; Schreier and Brown, 2001; Renschler, 2003). A GIS stores spatial data, determines model parameters, provides scale-independent visualizations, and allows analysis and combination of maps from various scales (Thieken et al., 1999). Geographic information systems have influenced the development and implementation of hydrologic models in several different ways. First, GIS has provided new opportunities to develop and run fully distributed models efficiently. These models take into account and predict the values of studied phenomena at any point within the watershed (Mitas and Mitasova, 1998). Second, GIS has also allowed users to run more traditional lumped models

more efficiently and to include at least some level of spatial effects by partitioning an entire watershed into smaller subwatersheds. Hellweger and Maidment (1999) automated a procedure to define and connect hydrologic elements in ARC/INFO and ArcView and write the results to an ASCII file that is readable by the Hydrologic Engineering Center's Hydrologic Modeling System (HEC-HMS). Third, GIS has been used to transform what were originally site-specific models into spatially distributed models. Finally, GIS is sometimes used to vary model inputs and compare model outputs with field data for improving the scientific process. Paniconi et al. (1999) reviewed the strengths and weaknesses of GIS and explained why distributed hydrologic models typically rely on GIS.

In this study we used the distributed modeling capability of GIS to apply a simple sequential data assimilation (i.e., EnKF) approach in conjunction with a numerically robust vadose zone hydrology model (i.e., HYDRUS-ET; Simunek et al., 1997) that incorporates periodic remotely sensed surface soil moisture observation (from a passive microwave remote sensor, ESTAR) to estimate root zone (profile) soil moisture. This newly developed soil moisture assessment tool (SMAT) has the advantage of combining the spatio-temporal continuity of the model prediction with intermittent input of remotely sensed observations in a geographically distributed framework to improve the root zone soil moisture estimation and minimize vadose zone model and parameter uncertainties using the data assimilation protocol.

MATERIALS AND METHODS

Study Watershed and Distributed Hydro-Climatic Parameters

The 603-km^2 LW watershed (Fig. 1) located in southwest Oklahoma in the Southern Great Plain region of the USA was selected for this study. The LW watershed was chosen because it has been the focus of several remote sensing experiments, including Washita92 (Jackson et al., 1995), Washita94, SGP97 (Jackson et al., 1999), SGP99, and Soil Moisture Experiment 2003, SMEX03 (Jackson et al., 2005). Specifically, we used the ESTAR L-band passive microwave radiometer, horizontally polarized at 1.413 GHz (0.21 m) with a bandwidth of 20 MHz. ESTAR was used to map soil moisture at a resolution of 800 by 800 m during the SGP97 experiment (Jackson et al., 1999). The detailed description of the SGP97 experimental plan and other supplementary information can be found at http://hydrolab.arsusda.gov/sgp97/ (verified 30 Dec. 2005).

Extensive meteorological networks (of USDA-ARS Micronet, Oklahoma Mesonet, DOE/NOAA) across the region provide good spatio-temporal distribution of hydrometeorological parameters. As used in this study, rain-gauges of the USDA-ARS Micronet are strategically located in the watershed at a spacing of approximately 5000 m. Forty-two of these stations continuously measure rainfall, solar radiation, air temperature, and relative humidity at 5-min intervals. At three stations, wind speed and barometric pressure are also recorded. There are 64 well-defined soil series in the LW watershed, with sand, loamy sand, sandy loam, loam, and silty loam being the predominant textures on the soil surface (Allen and Naney, 1991). Land use and land cover (LULC) is dominated by rangeland/pasture (63%), with significant areas of winter wheat (*Triticum aestivum* L.) and other crops mostly in the flood plains and western portion of the watershed. The topography of the region is moderately rolling with a maximum relief of <200 m.

All the relevant GIS data used in this study, including soil properties, land cover, and remotely sensed surface soil moisture, were derived from the SGP97 database available at http://www.cei.psu.edu/nasa_lsh/ (verified 30 Dec. 2005). The meteorological data (i.e., daily precipitation, wind speed, relative humidity, air temperature, and solar radiation) used in this study were derived from ftp://daac.gsfc.nasa.gov/data/sgp97/ (verified 30 Dec. 2005). The footprint size of ESTAR-based soil moisture (800 by 800 m) was used as the basis for grid resampling for all variables, resulting in a total of 843 pixels across the LW watershed. The soil textural distribution (Fig. 2) of LW has five dominant soil types: silty loam (32%), sandy loam (29%), loam (10.4%), sand (8.8%), and loamy sand (18%). During SGP97, the LULC grid (Fig. 3) had four main land cover types: pasture, corn (*Zea mays* L.), wheat, and

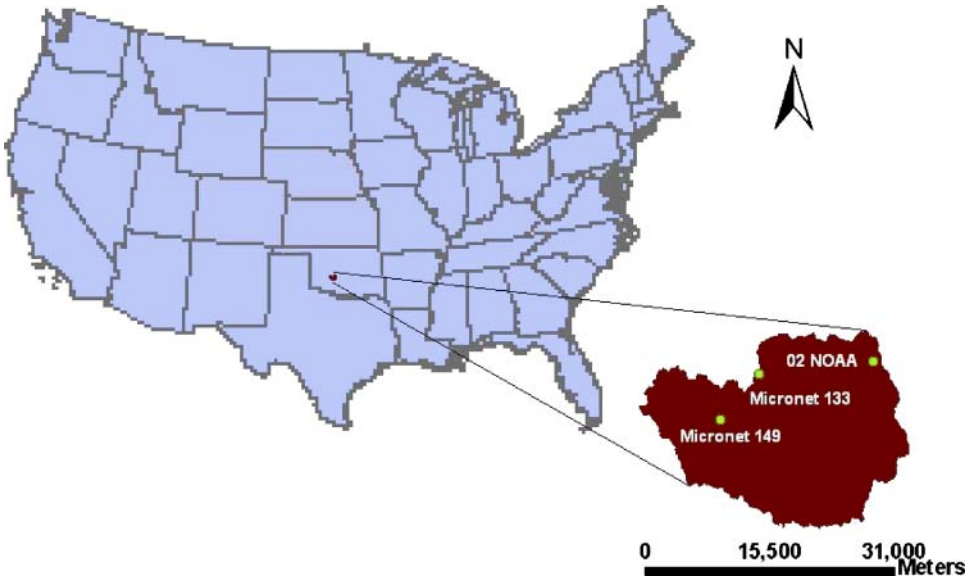

Fig. 1. Little Washita (LW) watershed with Micronet and NOAA sites used in the study.

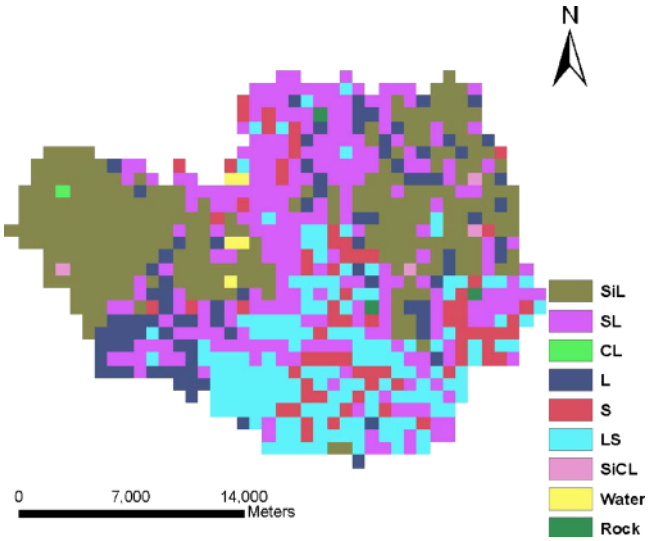

Fig. 2. Little Washita (LW) watershed soil map resampled at a resolution of 800 by 800 m. SL, sandy loam; SiL, silty loam; L, loam; Cl, clay; CL, clay loam; S, sand; SiCL, silty clay loam.

alfalfa (*Medicago sativa* L.). Average values of daily wind speed, relative humidity, and solar radiation based on all Micronet stations across the watershed were used for the model simulations. Micronet-based daily total precipitation data for the entire duration of SGP97 experiment (18 June–16 July 1997) were spatially interpolated and resampled at 800 by 800 m resolution.

The resulting daily spatially distributed hydroclimatic data sets were used as inputs to the HYDRUS-ET model. Other necessary distributed model inputs such as leaf area index, albedo, and surface roughness across the LW watershed were from Jackson et al. (1999). Knowledge of soil hydraulic properties is a key input for root- and vadose-zone hydrologic modeling. Laboratory and field methods for determining soil hydraulic properties across large land areas are time-consuming and expensive. Average soil hydraulic properties based on soil texture (i.e., pedotransfer functions) are commonly used in hydrologic models. In this study, the average values for selected soil water retention and hydraulic conductivity parameters for the major soil textural classes by Carsel and Parrish (1988) (Table 1) were used. Local (point) profile soil moisture data measured at three Micronet sites (Heathman et al., 2003) highlighted in Fig. 1 were used for comparison and validation with the model–data assimilation outputs at the pixel scale.

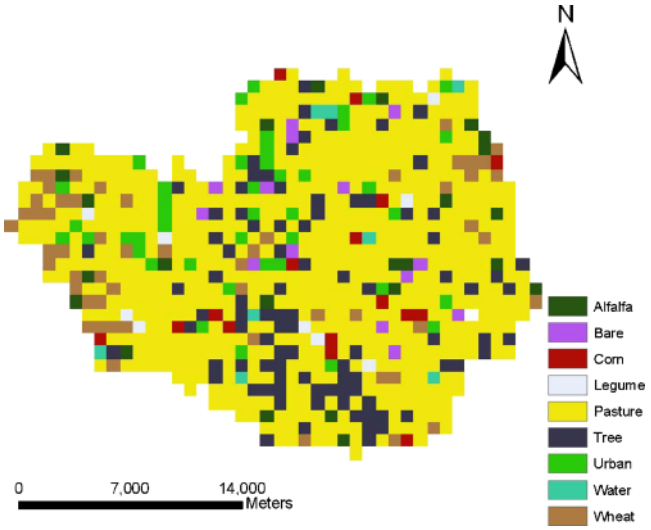

Fig. 3. Land use land cover (LULC) for Little Washita (LW) watershed resampled at a resolution of 800 by 800 m.

Table 1. Average hydraulic properties for different soil textures (Carsel and Parrish, 1988).†

Texture	θ_r	θ_s	α	n	K_{sat}
			cm^{-1}		$m\ d^{-1}$
Sand	0.045	0.43	0.145	2.68	7.128
Loamy sand	0.057	0.41	0.124	2.28	3.502
Sandy loam	0.065	0.41	0.075	1.89	1.061
Loam	0.078	0.43	0.036	1.56	0.249
Silt	0.034	0.46	0.016	1.37	0.06
Silt loam	0.067	0.45	0.02	1.41	0.108
Sandy clay loam	0.1	0.39	0.059	1.48	0.314
Clay loam	0.095	0.41	0.019	1.31	0.062
Sandy clay	0.1	0.38	0.027	1.23	0.028
Silty clay	0.07	0.36	0.005	1.09	0.005
Clay	0.068	0.38	0.008	1.09	0.048

† θ_r, residual water content; θ_s, saturated water contents; α and n, fitting parameters related to particle-size distribution; K_{sat}, saturated hydraulic conductivity.

Soil Moisture Assessment Tool

The information flow for SMAT developed in this study to assess spatiotemporal distribution of profile soil moisture is presented in Fig. 4. The simplified distributed modeling system was primarily based on running the one-dimensional partially saturated vadose zone flow model HYDRUS-ET (Simunek et al., 1997) for each remote sensing footprint or pixel (800 by 800 m) without any pixel-to-pixel interaction within the ArcGIS framework. A major advantage of this GIS-based tool is its capability to automatically read and write (I/O) the spatially distributed input data (e.g., soil, LULC, precipitation, and initial ensemble for each time step) and execute the HYDRUS-ET model in every pixel. The toolbox also writes the mean results of the updated ensemble according to their geospatial coordinates.

We set up the one-dimensional HYDRUS-ET model for 843 ESTAR footprints–pixels across the LW watershed. The distributed footprint-scale parallel noninteracting stream tubes (soil columns–hydrologic units) were identified on a pixel basis with top or bottom boundary conditions, initial profile soil moisture conditions, and soil and land parameters. An interface program was developed in Microsoft Visual Basic 6.0 using Arc Objects to couple ArcGIS 9 with HYDURS-ET and EnKF using a C subroutine (Dynamic Link Library). The

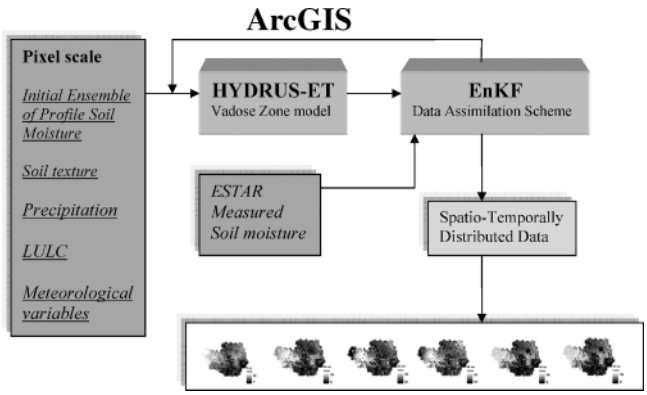

Fig. 4. Schematic representation of the Soil Moisture Assessment Tool (SMAT).

integrated model reads pixel-wise input information (e.g., soil texture, LULC, precipitation) from the GIS grids and assigns parameters, boundary conditions, and initial conditions in the input files of HYDRUS-ET. Other specifications and assumptions for our model simulation runs are given in Table 2. Soil profiles of 0.65-m thickness were considered, with atmospheric top boundary and free draining bottom boundary. The soil profile was discretized into 97 elements (ranging from 0.001 to 0.1 m) with finer discretization near the land–atmosphere boundary where a large hydraulic gradient was expected as compared with the deeper depths. Time-dependent top boundary conditions were used with precipitation distribution across the LW watershed. A unit (vertical) hydraulic gradient (free drainage) condition was used at the bottom boundary of the root zone for all the pixels. The spatial correlation of the uncertain initial soil profile input is unknown a priori and difficult to characterize. Porosity and wilting point control the upper and lower limit of volumetric soil moisture, respectively. The saturated hydraulic conductivity, which is highly variable in space, is a primary factor affecting infiltration. So, the initial status of soil moisture in the discretized soil profile is assigned a uniform value of 50% of the relative saturation according to soil type and texture. For computational limitations and efficiency 100 replicates were populated in the ensemble with a Gaussian noise of 20 to 5% of the soil moisture in decreasing order from top to bottom of the soil profile. Reichle et al. (2002) and Crow and Wood (2003) demonstrated with synthetic test problems that an ensemble of 100 replicates is sufficiently large to provide accurate estimates of soil moisture for the SGP conditions.

Due to the lack of physical data and for computational simplicity, we assumed: (i) only one soil texture per pixel for the entire root zone (i.e., the soil texture at the soil surface was assigned for the whole 0.65-m depth of the soil profile); (ii) pixels with rock outcrop, urban, and water cover were excluded in the simulation; (iii) any excess water above the soil surface was immediately removed; and (iv) runoff and runon between adjacent pixels due to surface topography were considered minimal, thus limiting the flow to the vertical direction only.

To assess the performance of the integrated SMAT model we conducted a simulation experiment based on the dataset of SGP97 Hydrology experiment for LW watershed (Jackson et al., 1999). The SMAT was run for the entire duration of the SGP97 remote sensing experiment ranging from Day of Year (DOY) 169 to 197 (18 June–16 July 1997) for profile soil moisture estimation on a daily time step. The dates when (ESTAR) measured soil moisture were not available, model forecast ensemble estimates were carried forward with time for the entire profile. Availability of (ESTAR) measured soil moisture to the model was made through analysis/update of the ensemble. Final state and measurement estimates were calculated by averaging the predictions made by the model replicates within the ensemble. After the completion of the data assimilation protocol for daily time steps, ensemble means were written to an output file and read into soil moisture grids at various depths across the watershed.

Table 2. Definition, values, and sources for the parameters used in HYDRUS-ET.

Parameter definition	Value
Number of soil layers	1
Thickness of soil zone	0.65 m
Soil hydraulic properties	Carsel and Parrish (1988)
Time step	daily
Heat flow	0
Solute flow	0
Root growth	0
Upper boundary	atmospheric
Bottom boundary	free drainage
Hysteresis	0
Number of Fixed nodes/elements across soil profile	97
Surface roughness	Jackson et al. (1999)
LAI†	Jackson et al. (1999)
Transpiration depth of all land cover	0.6 m (below top 0.05 m)
Wind speed	avg. wind speed of watershed
Ambience temperature	avg. temperature of watershed,
Relative humidity	avg. relative humidity of watershed

† LAI, leaf area index.

Brief Description of HYDRUS-ET and Governing Equations

HYDRUS-ET is a numerical model with a Galerkin-type linear finite-element scheme that solves the Richards' equation for partially saturated water flow. The one-dimensional water movement in a partially saturated rigid porous medium is described by a modified form of Richards' equation using the assumption that the air phase plays an insignificant role in the liquid-flow process and that the water flow due to thermal gradient can be neglected:

$$\frac{\partial \theta}{\partial t} = \frac{\partial}{\partial x}\left[K\left(\frac{\partial h}{\partial x} + \cos\beta\right)\right] - S \qquad [1]$$

where h is the soil water pressure head (m), θ is the volumetric water content ($m^3\ m^{-3}$), t is the time (s), x is the spatial coordinate (m), S is the sink term ($m^{-3}\ s^{-1}$), β is the angle between the flow and the vertical axis, and K is the unsaturated hydraulic conductivity function ($m\ s^{-1}$) given by

$$K(h,x) = K_s(x)K_r(h,x) \qquad [2]$$

where K_r is the relative hydraulic conductivity and K_s is the saturated hydraulic conductivity. The unsaturated soil hydraulic properties, $\theta(h)$ and $K(h)$, generally highly nonlinear functions of pressure head, were described by van Genuchten (1980):

$$\theta(h) = \theta_r + \frac{\theta_s - \theta_r}{[1 + (\alpha h)^n]^{1-\frac{1}{n}}} \qquad [3]$$

where $\theta(h)$ represents the water retention curve defining the water content, θ ($m^3\ m^{-3}$), as a function of the soil water pressure head h (m), θ_r and θ_s ($m^3\ m^{-3}$) are residual and saturated water contents, respectively, while α (m^{-1}) and n are fitting parameters related to particle-size distribution. Equation [3] is used in conjunction with the pore-size distribution model by Mualem (1976) to yield the hydraulic conductivity function (van Genuchten, 1980):

$$K(S_e) = K_o S_e^l\{1 - [1 - S_e^{n/(n-1)}]^{1-1/n}\}^2 \qquad [4]$$

where K_o is the matching point at saturation ($m\ s^{-1}$), and parameter l is an empirical pore tortuosity–connectivity parameter. The model considers prescribed water flux at the top and bottom boundaries across the root zone determined by atmospheric conditions or free drainage. The Penman method was used to calculate daily evapotranspiration using two steps: (i) calculate the potential evapotranspiration and (ii) calculate the actual evapotranspiration rate using a relationship between relative evapotranspiration and the pressure head, h, along the soil profile.

Ensemble Kalman Filter

Data assimilation systems are typically designed to merge uncertain predictions from models with incomplete and noisy

measurements from an observing system. Assimilation approaches optimally combine model predictions and independent observations in such a manner that the shortcomings of each approach are mutually compensated. Evensen (2003) presented an algorithm based on an ensemble of model predictions to evaluate error covariance information necessary for the standard Kalman Filter for updating model predictions using observations. The method uses a nonlinear model to propagate the ensemble state across space or time. The initial ensemble was chosen to properly represent the soil profile error statistics by adding perturbation (Gaussian distributed noise) to the initial guess of the model states. The resulting ensemble reflects the uncertainty introduced by input errors. The ensemble replicates a broad range of values and the variances of the propagated states increase, as compared with the case where model input values are held fixed at their nominal values. This increased variability across the ensemble tends to make the filter rely more on measurements and reduces the adverse impact of model bias. We used an ensemble size of 100 in the application described here. It uses the physics of the vadose zone model (HYDRUS-ET) to vertically extrapolate surface soil moisture measurements to soil moisture states at deeper depths not directly observed by the remote sensor. The nonlinear one-dimensional vadose zone model used for assimilation can be represented in a generic form as the spatially discretized soil moisture at all computational nodes across the soil profile at time t into a state vector ψ of dimension n (Reichle et al., 2002):

$$\frac{\mathrm{d}\boldsymbol{\psi}}{\mathrm{d}t} = F(\boldsymbol{\psi}) + \omega \qquad [5]$$

The nonlinear operator $F()$ includes all deterministic forcing data (e.g., observed rainfall). Uncertainties related to the errors in the model or the forcing data are summarized in ω. The observations used for the assimilation scheme are remotely sensed (ESTAR) measurements of soil moisture across the LW watershed during the SGP97 experiment (Jackson et al., 1999). The ensemble of model state is integrated forward in time according to Eq. [1]. The matrix of the forecast ensemble members can be written as:

$$\mathbf{A} = (\psi_1, \psi_2, \psi_3, \ldots, \psi_N) \in \Re^{n\times N} \qquad [6]$$

where N is the number of ensemble members and n is the size of the model state vector. The ensemble-mean matrix ($\overline{\mathbf{A}}$) can be defined as

$$\overline{\mathbf{A}} = \mathbf{A}1_N \qquad [7]$$

where $1_N \in \Re^{N\times N}$ is a matrix in which each element is equal to $1/N$. The ensemble perturbation matrix can then be defined as

$$\mathbf{A}' = \mathbf{A} - \overline{\mathbf{A}} \qquad [8]$$

The ensemble covariance $\mathrm{P_e} \in \Re^{n\times n}$ can be defined as

$$P_\mathrm{e} = \frac{\mathbf{A}'(\mathbf{A}')^T}{N-1} \qquad [9]$$

For example, at time t_i over the region of interest, we possess an ensemble of forecasts that are representative of the true state of soil moisture. Typically, the ensemble-mean forecast is the best prediction of the profile soil moisture state at t_i. Now if we receive an ESTAR-based soil moisture observation at the same time t_i, then we need to update our prediction of the soil moisture state and its uncertainty given this new observation. While the observation carries information about the surface soil moisture state only, we intend to extract information about the entire soil moisture profile. Thus, the representative forecast ensemble was used to derive polynomial coefficients between surface and subsurface computational nodes present in the state vector ($\mathbf{A}$) by using a least squares fit. These polynomials were then used to calculate the observed state vector of measurement ensemble by adding perturbation (Gaussian distributed noise). Given a vector of observation $\mathbf{d}$,

$$\mathbf{D} = (d_1, d_2, d_3, \ldots, d_n) \in \Re^{n\times N} \qquad [10]$$

The perturbation matrix of $\mathbf{D}$ is defined by

$$X \in \Re^{n\times N} \qquad [11]$$

from which we construct the ensemble of the covariance matrix

$$R_\mathrm{e} = \frac{XX^T}{N-1} \qquad [12]$$

The updated equation, expressed in terms of ensemble covariance matrices, is

$$\mathbf{A}^a = \mathbf{A} + P_\mathrm{e}\mathbf{H}^T(\mathbf{H}P_\mathrm{e}\mathbf{H}^T + R_\mathrm{e})^{-1}(\mathbf{D} - \mathbf{HA}) \qquad [13]$$

where $\mathbf{A}^a$ is the updated matrix, ($\mathbf{D} - \mathbf{HA}$) is the innovation matrix, $P_\mathrm{e}\mathbf{H}^T$ ($\mathbf{H}P_\mathrm{e}\mathbf{H}^T + R_\mathrm{e})^{-1}$ is the Kalman gain, and $\mathbf{H}$ interpolates the true state (i.e., ESTAR based brightness temperature) of the observed quantity (i.e., soil moisture). In this case $\mathbf{H}$ is an identity matrix because the soil moisture product of ESTAR was used directly instead of microwave brightness temperature. The analyzed, updated matrix $\mathbf{A}^a$ is carried forward in time as ensemble of initial state for the next time step.

Statistical Methods

To evaluate the performance of the proposed data assimilation scheme with respect to the point measurements of profile soil moisture, we used coefficient of determination (R^2), root mean square error (RMSE), and mean bias error (MBE). The statistics of RMSE and MBE are defined as

$$\mathrm{RMSE} = \sqrt{\frac{\sum(P-O)^2}{n}} \qquad [14]$$

$$\mathrm{MBE} = \frac{\sum(P-O)}{n} \qquad [15]$$

where P and O are predicted and observed soil moisture, respectively, and n is the number of observations. The RMSE and MBE are indicative of overall error and mean bias in the estimation process, respectively.

RESULTS AND DISCUSSION

Performance of the SMAT was evaluated by comparing the simulated (overlapping) footprint-scale profile soil moisture to the local (point-scale) profile soil moisture data measured at three Micronet sites (Heathman et al., 2003), which are highlighted in Fig. 1. These three sites (i.e., Micronet-133, Micronet-149, and 02-NOAA) were selected for validation because they represent typical scenarios in the LW watershed.

Site Micronet-133

Site Micronet-133 was selected due to the matching soil profile (based on pixel-scale NRCS soil database, Fig. 2) used in the model and the local (point-scale) observation at the field site. Point observations indicate

a sandy loam soil for the entire soil profile, which agrees with our model assumption of the soil texture at the soil surface assigned for the whole soil profile depth of 0.65 m. Figure 5a shows the surface soil moisture comparison between models without data assimilation (Open-loop) and with EnKF-based data assimilation, and ESTAR observations at the top 0- to 5-cm depth. Open loop results are obtained from the average of 100 replicates without updating. Figure 5a illustrates the ability of EnKF to correct the errors in HYDRUS-ET model estimations. Figures 5b through 5d show the comparison of SMAT-based profile soil moisture estimations and TDR-based field observations at four different depths. From DOY 170 to 175 the root zone soil moisture estimated by the model at the depths of 0 to 0.15, 0.15 to 0.30, and 0.45 to 0.60 m depends on the initial estimate of the ensemble. The filter improved the surface soil moisture at the initial period of the simulation, in contrast to the soil moisture at the deeper depths. The continuous analysis–update (i.e., EnKF-based assimilation of surface soil moisture using ESTAR observations) from DOY 175 to 184 (except on 179) improved the profile soil moisture estimations, and the trends of the simulated and observed states matched well. These matching trends in Fig. 5b through 5d verify the hypothesis that surface soil moisture observation obviously carries information about the unobserved portion of the state (profile soil moisture). Even after the gap in ESTAR overflights between DOY 184 and 192 the model maintains a good trend except on DOY 191. On DOY 191, the impact of a rainfall event is clearly visible in the model estimates, but was missing in the measured soil moisture at the depth of 0 to 0.15 m (Fig. 5b). This emphasizes the importance and sensitivity of the precipitation information available to the model at a daily time step, which affects the performance of the model. The filter regained the trend from DOY 193 due to new ESTAR measurements from DOY 193 to 197 except on DOY 196. Statistical comparison of the model estimations with point measurements is given in Table 3. For this site high R^2 values were observed for all the depths across the root zone, indicating the efficient data assimilation capability of SMAT for surface soil moisture reaching to the deeper depths under favorable conditions (i.e., for matching soil profile at the pixel- and point-scales). Low RMSE values observed for this site confirm the suitability of the model and agreement of assumptions with field conditions.

Site Micronet-149

The actual soil profile (based on point observations) of this site matches the model soil profile of silty loam for the top 0.30 m (Table 3). Figure 6a shows the surface (0–5 cm) soil moisture comparison of the Open-loop, model with EnKF, and ESTAR observations. As expected, the Open-loop and EnKF predictions drift apart, and ESTAR measured soil moisture allow the EnKF to capture the dry-down portion of the experiment (DOY 170–185). Uncertainty in hydraulic parameters and bot-

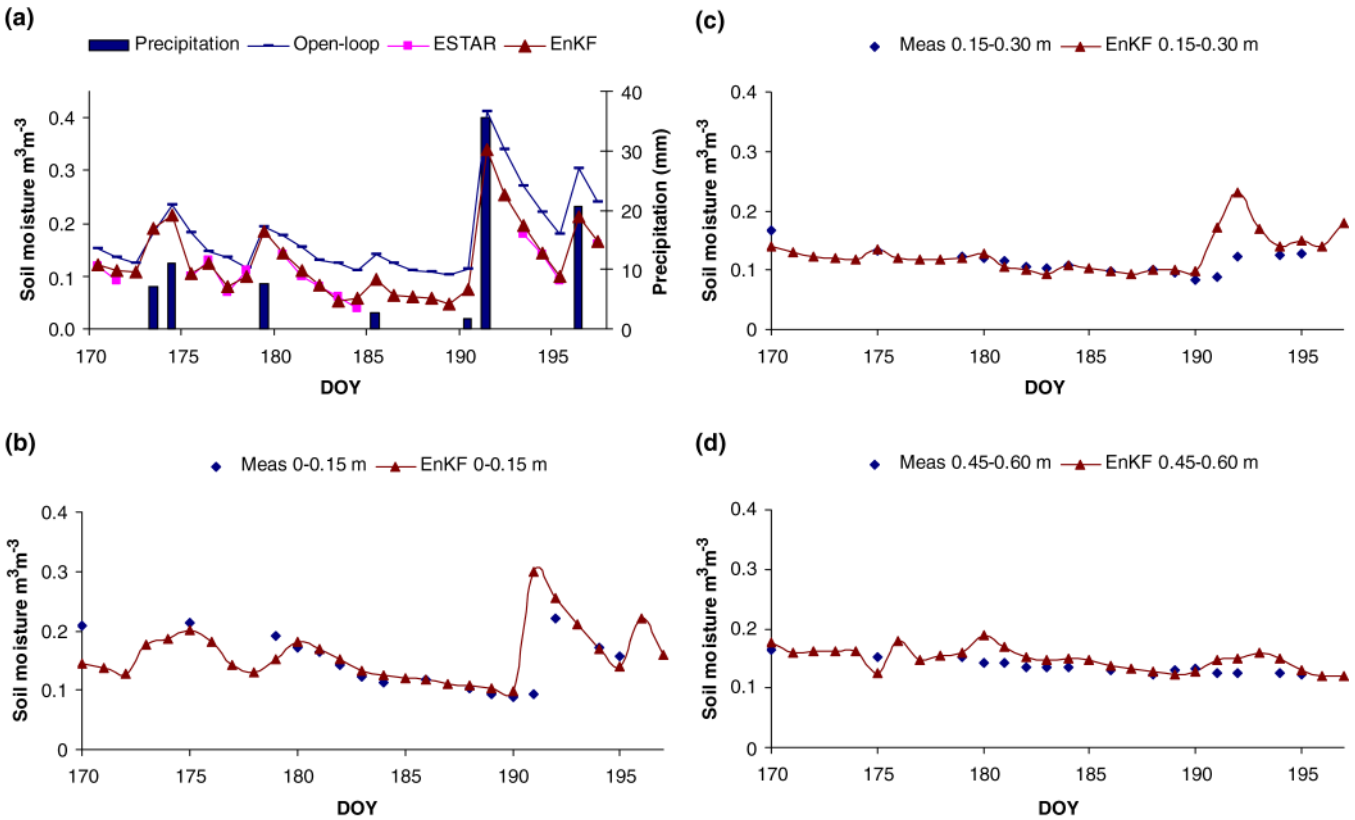

Fig. 5. Site Micronet-133 temporal series of soil moisture at (a) surface, (b) 0 to 0.15 m, (c) 0.15 to 0.30 m, and (d) 0.45 to 0.60 m. DOY, day of year; EnKF, ensemble Kalman filter; Meas, measured.

Table 3. Comparison of field soil moisture measurements and model results from Day of Year (DOY) 170 to 197 at 02-NOAA, Micronet-133, and Micronet-149.†

Sites	Statistics	0–0.15 m	0.15–0.30 m	0.30–0.45 m	0.45–0.60 m
Micronet-133	Local	SL	SL	SL	SL
	Model	SL	SL	SL	SL
	R^2	0.82	0.84	0.88	0.79
	MBE	−0.0052	0.0014	−0.007	0.01
	RMSE	0.0048	0.0057	0.0002	0.002
Micronet-149	Local	SiL	SiL	L	CL
	Model	SiL	SiL	SiL	SiL
	R^2	0.81	0.67	0.25	0
	MBE	0.0029	−0.0715	−0.0847	−0.1129
	RMSE	0.012	0.0065	0.0261	0.0392
02-NOAA	Local	L	Cl	L	SiL
	Model	SL	SL	SL	SL
	R^2	0.55	0.3	0.23	0.15
	MBE	−0.1034	−0.1674	−0.1697	−0.1697
	RMSE	0.0174	0.0342	0.0394	0.0398

† SL, sandy loam; SiL, silty loam; L, loam; Cl, clay; CL, clay loam.

tom boundary conditions and the mismatch of soil profile below 0.30 m were the limiting factors for the model. The bottom-most clay layer in the actual soil profile restricted the downward flux during the experiment and retained higher moisture in the soil profile between 0.30 and 0.60 m. The higher K_s value of silt loam (Table 1) compared with the clay loam layer considered in the model drained the soil profile faster during the simulation, resulting in lower soil moisture predictions. The EnKF algorithm failed to maintain the temporal trends at the deeper layers (except the surface moisture) due to imperfect forecast ensemble polynomial coefficients obtained by least squares fit. Figures 6b through 6d illustrate the comparison of profile soil moisture using the data assimilation scheme (SMAT) and field-observed values at the depths of 0 to 0.15, 0.15 to 0.30, and 0.45 to 0.60 m. Of particular significance, the EnKF estimates for soil profile at the 0- to 0.15-m depth closely matched the point-scale measurements (Fig. 6a), with R^2, MBE, and RMSE values of 0.81, 0.0029, and 0.01, respectively (Table 3). Even though the profile soil texture at the 0.15- to 0.30-m depth in the model and at the field location were the same, observed and estimated soil moistures at this depth did not match well

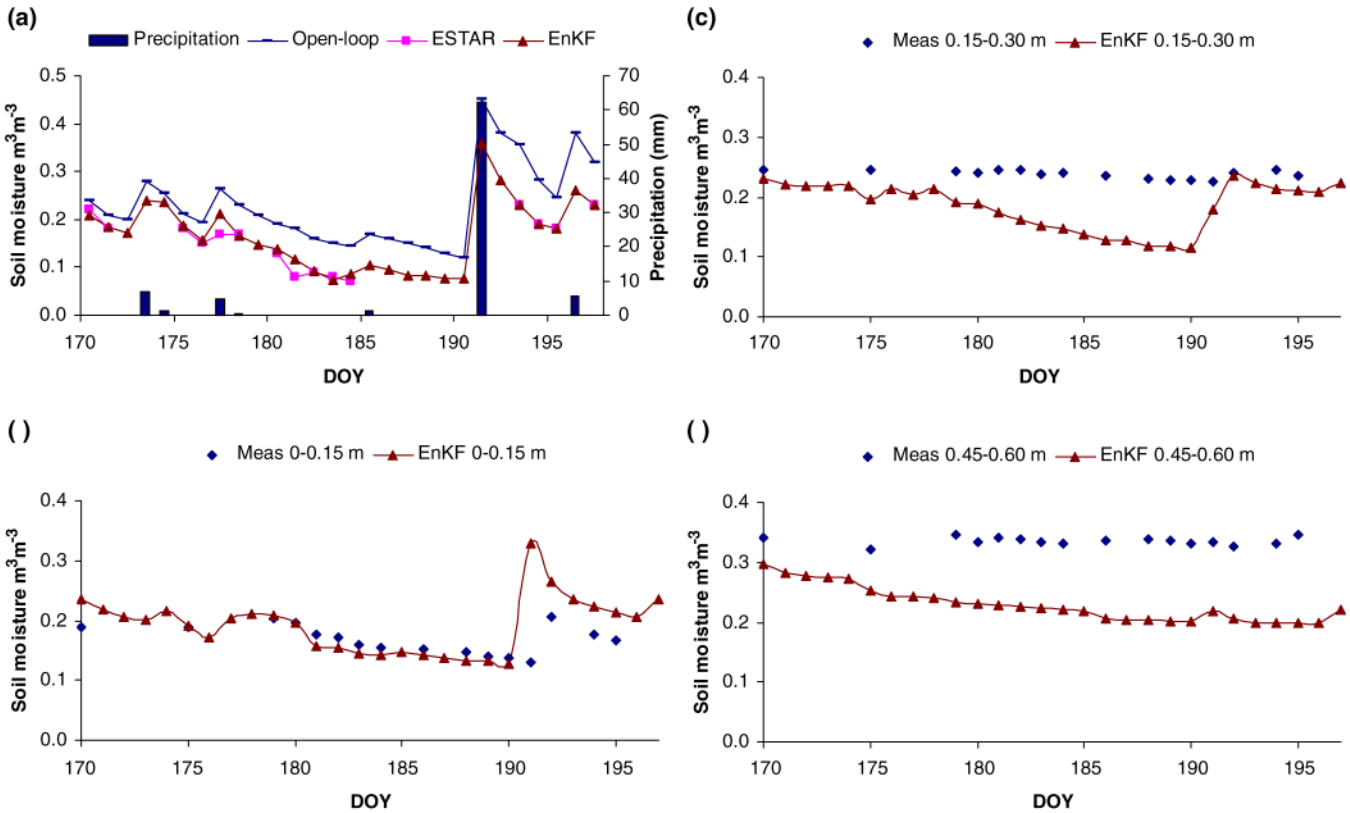

Fig. 6. Site Micronet-149 temporal series of soil moisture at (a) surface, (b) 0 to 0.15 m, (c) 0.15 to 0.30 m, and (d) 0.45 to 0.60 m. DOY, day of year; EnKF, ensemble Kalman filter; Meas, measured.

(see Fig. 6c) due to the impact of the clay loam layer at the bottom of the profile. The filter totally underestimated the soil moisture in the deeper zone (0.45–0.60 m), with a MBE of −0.1129 (Table 3). At the field site, however, the clay layer retains moisture at an average 0.35 m^3 m^{-3} throughout the observation period due to the impeding layer.

Site 02-NOAA

This site was especially chosen to demonstrate the impact of a total mismatch of the model soil profile with the local soil profile (Table 3), which completely alters the flow regime of the soil column by introducing uncertainty in hydraulic parameters. The model used sandy loam for the entire 0- to 0.60-m soil profile, which led to a well-drained soil column for this site. Neither the Open-loop nor the EnKF could predict the local soil moisture at this site. As evident from Fig. 7b through 7d, no agreement between measurement and EnKF was observed at any depth, with high negative bias for the entire root zone (Table 3). Note, however, EnKF could update the surface (0–5 cm) soil moisture prediction across the study period (Fig. 7a). A partial agreement was observed at the depth of 0 to 0.15 m following the rainfall event on DOY 191.

The duration of the SGP97 hydrology experiment was comparatively shorter than what is generally applied to models. It is not apparent whether a shorter period had any appreciable effect on the model results, although some previous studies have found that soil moisture predictability may be related to the model time scale (e.g., Schlosser and Milly, 2000). At all three study sites (02-NOAA, Micronet-133, and Micronet-149) in the early part of the experiment (first 10 d) EnKF-estimated soil moisture on the surface was only marginally better than the Open-loop (Fig. 5a, 6a, 7a). Margulis et al. (2002) found similar results at the watershed and regional scales. For sites Micronet-133, Micronet-149, and 02-NOAA, Open-loop and EnKF for soil surface lead to RMSE values of 0.062, 0.090, 0.054 and 0.010, 0.013, 0.011, respectively. Figures 5a, 6a, and 7a confirm that EnKF is able to track the dry-down period after precipitation events much better than the Open-loop modeling scheme. A significant benefit of the EnKF in the proposed integrated model is its ability to instantaneously update moisture estimates and error standard deviations throughout the soil profile. This is possible due to the carry-over memory of the surface soil moisture to the profile soil moistures. As discussed for the site Micronet-133, the effects of surface moisture update on the profile soil moistures only become evident gradually with time, as surface moisture variations redistribute throughout the soil profile (Fig. 5b–5d).

Precipitation is the most important time-dependent forcing data for soil moisture distribution in hydrologic studies (Margulis et al., 2002). Precipitation uncertainties, especially in ungauged areas, can be expected to have significant impact on the evolution and distribution of soil moisture. A major limitation of SMAT is the

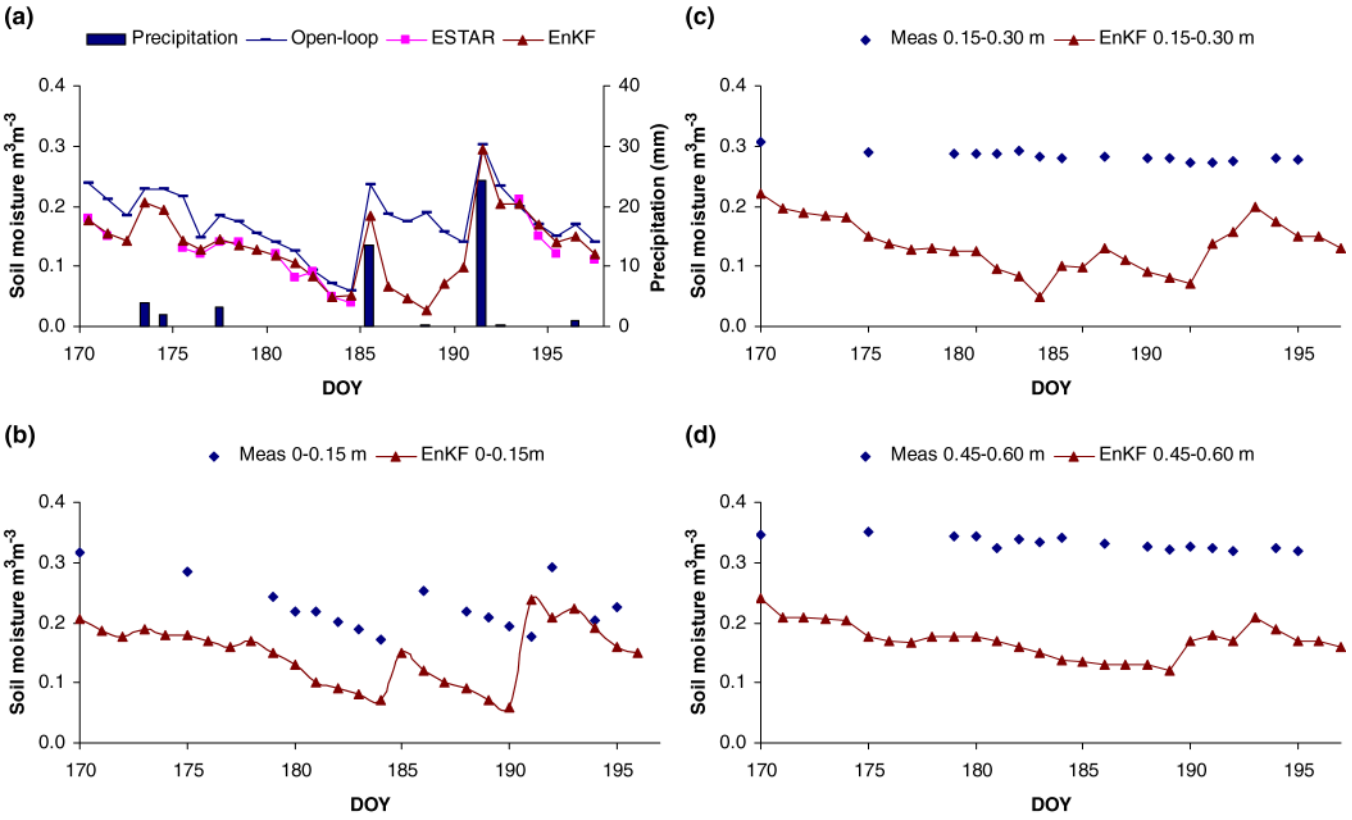

Fig. 7. Site 02-NOAA temporal series of soil moisture at (a) surface, (b) 0 to 0.15 m, (c) 0.15 to 0.30 m, and (d) 0.45 to 0.60 m. DOY, day of year; EnKF, ensemble Kalman filter; Meas, measured.

implications of deterministic forcing data, mainly precipitation. At the three study sites (02-NOAA, Micronet-133, and Micronet-149), the peak surface soil moistures were observed after a day from the model estimation peak on DOY 191. This lagged behavior in surface soil moisture could partially be due to the use of daily (24-h cumulative) precipitation values reported for the following day. Subsequently, lagging surface soil moisture adversely affects the filter performance when comparing the results with the local point profile data for a particular day. Another limitation that affects the model performance of EnKF is the assumption of one soil texture across the whole depth of the soil profile. Soil hydraulic parameters for sandy loam and silty loam profiles of sites 02-NOAA and Micronet-149, respectively, in the model are much different from the local soil profiles. Furthermore, the spatial variability of soil hydraulic conductivity and soil water retention characteristics across the corresponding (ESTAR) remote sensing pixel greatly influence the vertical and lateral soil moisture transmission. The effect of soil texture was further illustrated by Mohanty and Skaggs (2001), who demonstrated the relationship of soil texture in determining soil moisture stability and variability across time at selected ESTAR remote sensing footprints during the SGP97 experiment. Inclusion of more detailed soil database or aggregated/effective soil hydraulic parameters (e.g., Zhu and Mohanty, 2002, 2003a, 2003b) for future applications of this distributed root zone SMAT may overcome this limitation.

Figure 8 shows the output of our ArcGIS-based distributed root zone process model with the EnKF data assimilation scheme (SMAT) in terms of soil moisture states across the LW watershed for DOY 193 (12 July 1997) at four discrete depths (0.05, 0.20, 0.40, and 0.60 m). The discussion of Sellers et al. (1995) about spatial heterogeneity introduced by rainfall and removed through dry-down dynamics is also applicable at this coarse (watershed) scale. During the dry-down period, the effect of soil texture (Fig. 2) on surface (0–5 cm) soil moisture patterns (Fig. 8) is visible at this scale, which matches with the findings of remote sensing observations across the SGP97 region (Jackson et al., 1999). A significant advantage of the ArcGIS-based SMAT is that it can be adopted at any fine or coarse spatial resolution to identify the transitional scale that separates (nonlinear) fine- versus coarse-scale soil moisture dynamics, where changes in soil moisture spatial heterogeneity are negatively or positively correlated with the change in mean soil moisture.

SUMMARY AND CONCLUSION

We developed a new distributed root zone soil moisture assessment tool (SMAT) on the ArcGIS platform by fully integrating a one-dimensional vadose zone hydrology model (HYDRUS-ET) with EnKF data assimilation capability using the parallel noninteracting stream tubes concept and remotely sensed surface soil moisture as the primary input. A major advantage of this novel scheme is that it can be used to compute root zone soil moisture distribution and its temporal evolution at multiple spatial resolutions including landscape, watershed, and regional scales. Results illustrate both the challenges and potential benefits of this new model. The system described here is formulated with its ultimate application in purview (i.e., operational estimation of near surface and root zone soil moisture using aircraft-/satellite-based microwave remote sensing measurements at different scales). Comparisons of EnKF filter simulations estimates with Open-loop simulations estimates

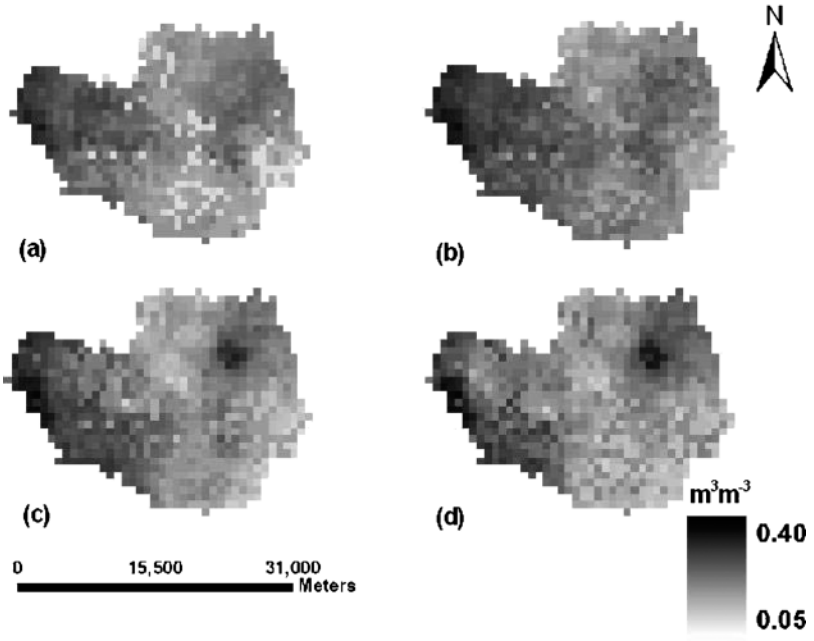

Fig. 8. Model-predicted soil moisture grids at different depths across Little Washita (LW) watershed Day of Year (DOY) 193 (12th July 1997) at the depth of (a) 0.05 m, (b) 0.2 m, (c) 0.4 m and (d) 0.6 m.

also demonstrate the advantage of assimilating remote sensing measurements with model estimations, which are consistent with previous studies at the SGP sites. Passive microwave-based soil moisture measurements are particularly important during the dry-down period when the Open-loop model may diverge. The model displayed a reasonable capability to generate soil moisture distribution at the desired resolution at various depths of the root zone in Little Washita watershed during the Southern Great Plains 1997 (SGP97) remote sensing experiment. To improve model performance several issues need to be addressed in the future including "effective" hydraulic parameters across spatial scales, developing subsurface soil properties databases using direct and indirect methods, implementing more appropriate vadose zone flow models at the landscape scale, correction of forcing data, and implementation on spatially correlated pixels.

ACKNOWLEDGMENTS

We acknowledge the support of a NASA fellowship (ESSF/03-000-0191), NASA grants (NAG5-11702), and NSF-SAHRA. We also thank Gary Heathman for sharing the profile soil moisture measurements from Micronet sites.

REFERENCES

Allen, P.B., and J.W. Naney. 1991. Hydrology of Little Washita river watershed, Oklahoma: Data and analyses. USDA Tech. Rep. ARS-90. USDA-ARS, Durant, OK.

Bindlish, R., W.P. Kustas, A.N. French, G.R. Diak, and J.R. Mecikalski. 2001. Influence of near-surface soil moisture on regional scale heat fluxes: Model results using microwave remote sensing data from SGP97. IEEE Trans. Geosci. Remote Sens. 39:1719–1728.

Camillo, P., and T.J. Schmugge. 1983. Estimating soil moisture storage in the root zone from surface measurements. Soil Sci. 135: 245–264.

Carsel, R.F., and R.S. Parrish. 1988. Developing joint probability distributions of soil water retention characteristics. Water Resour. Res. 24:755–769.

Chen, F., K. Mitchell, J. Schaake, Y. Xue, H.L. Pan, V. Koren, Q.Y. Duan, M. Ek, and A. Betts. 1996. Modeling of land-surface evaporation by four schemes and comparison with FIFE observations. J. Geophys. Res. 101:7251–7268.

Crosson, W.L., C.A. Laymon, R. Inguva, and M.P. Schamschula. 2002. Assimilating remote sensed data in a surface flux-soil moisture model. Hydrol. Processes 16:1645–1662.

Crow, W.T., and E.F. Wood. 2003. The assimilation of remotely sensed soil brightness temperature imagery into a land surface model using Ensemble Kalman Filtering: A case study based on ESTAR measurements during SGP97. Adv. Water Resour. 26:137–149.

Dai, Y., X. Zeng, R.E. Dickinson, I. Baker, G.B. Bonan, M.G. Bosilovich, A.S. Denning, P.A. Dirmeyer, P.R. Houser, G. Niu, K.W. Oleson, C.A. Schlosser, and Z.-L. Yang. 2003. The Common Land Model (CLM). Bull. Am. Meteorol. Soc. 84:1013–1023.

Dunne, S., and D. Entekhabi. 2005. An ensemble-based reanalysis approach to land data assimilation. Water Resour. Res. 41:W02013. doi:10.1029/2004WR003449.

Engman, E.T., and R.J. Gurney. 1991. Remote sensing in hydrology. Chapman and Hall, London.

Entekhabi, D., H. Nakamura, and E.G. Njoku. 1994. Solving the inverse-problem for soil moisture and temperature profiles by sequential assimilation of multifrequency remotely sensed observations. IEEE Trans. Geosci. Remote Sens. 32:438–448.

Evensen, G. 2003. The Ensemble Kalman filter: Theoretical formulation and practical implementation. Ocean Dyn. 53:343–367.

Famiglietti, J.S., J.A. Devereux, C.A. Laymon, T. Tsegaye, P.R. Houser, T.J. Jackson, S.T. Graham, and M. Rodell. 1999. Ground-based investigation of soil moisture variability within remote sensing footprints during the Southern Great Plains 1997 (SGP97). Hydrology experiment. Water Resour. Res. 35:1839–1851.

Georgakakos, K.P. 1996. Soil moisture theories and observations (special issue). J. Hydrol. 184:131–152.

Hanson, J.D., K.W. Rojas, and M.J. Schaffer. 1999. Calibrating the root zone water quality model. Agron. J. 91:171–177.

Hook, W.R., and N.J. Livingston. 1996. Errors in converting time domain reflectometry measurements of propagation velocity to estimates of soil water content. Soil Sci. Soc. Am. J. 60:35–41.

Hellweger, F.L., and D.R. Maidment. 1999. Definition and connection of hydrologic elements using geographic data. J. Hydraul. Eng. 4: 10–18.

Heathman, G.C., P.J. Starks, L.R. Ahuja, and T.J. Jackson. 2003. Assimilation of surface soil moisture to estimate profile soil water content. J. Hydrol. 279:1–17.

Houser, P.R., W.J. Shuttleworth, J.S. Famiglietti, H.V. Gupta, K.H. Syed, and D.C. Goodrich. 1998. Integration of soil moisture remote sensing and hydrologic modeling using data assimilation. Water Resour. Res. 34:3405–3420.

Jackson, T.J. 1993. Measuring surface soil moisture using passive microwave remote sensing. Hydrol. Processes 7:139–152.

Jackson, T.J., R. Bindlish, A.J. Gasiewski, B. Stankov, M. Klein, E.G. Njoku, D. Bosch, T.L. Coleman, C. Laymon, and P.J. Starks. 2005. Polarimetric scanning radiometer C and X band microwave observations during SMEX03. IEEE Trans. Geosci. Remote Sens. 43: 2418–2430.

Jackson, T.J., D.M. Le Vine, A.Y. Hsu, A. Oldak, P.J. Starks, C.T. Swift, J.D. Isham, and M. Hakan. 1999. Soil moisture mapping at regional scales using microwave radiometry: The Southern Great Plains hydrology experiment. IEEE Trans. Geosci. Remote Sens. 37: 2136–2151.

Jackson, T.J., D.M. Le Vine, C.T. Swift, T.J. Schmugge, and F.R. Schiebe. 1995. Large scale mapping of soil moisture using the ESTAR passive microwave radiometer in Washita '92. Remote Sens. Environ. 53:27–37.

Jackson, T.J., and T.J. Schmugge. 1989. Passive microwave remote sensing system for soil moisture: Some supporting research. IEEE Trans. Geosci. Remote Sens. GE-27:35–46.

Koster, R.D., and P.C.D. Milly. 1997. The interplay between transpiration and runoff formulations in land surface schemes used with atmospheric models. J. Clim. 10:1578–1594.

Koster, R., and M. Suarez. 1996. Energy and water balance calculation in the mosaic LSM. Technical Memorandum 1046069. NASA GSFC, Greenbelt, MD.

Kostov, K.G., and T.J. Jackson. 1993. Estimating profile soil moisture from surface layer measurement—A review. SPIE 1941:125–136.

Kustas, W.P., T.J. Jackson, A.N. French, and J.I. MacPherson. 2001. Verification of patch- and regional-scale energy balance estimates derived from microwave and optical remote sensing during SGP97. J. Hydrometeorol. 2(3):254–273.

Lachassagne, P., R. Wyns, P. Berard, T. Bruel, L. Chery, T. Coutand, J.-F. Desprats, and P. Le Strat. 2001. Exploitation of high-yields in hard-rock aquifers; downscaling methodology combining GIS and multicriteria analysis to delineate field prospecting zones. Ground Water 39:568–581.

Liang, X., E.F. Wood, and D.P. Lettenmaier. 1996. Surface soil moisture parameterization of the VIC-2L model: Evaluation and modifications. Global Planet. Change 13:195–206.

Margulis, S.A., D. McLaughlin, D. Entekhabi, and S. Dunne. 2002. Land data assimilation and estimation of soil moisture using measurements from the Southern Great Plains 1997 Field Experiment. Water Resour. Res. 38:1299–1317.

Mitas, L., and H. Mitasova. 1998. Distributed soil erosion simulation for effective erosion prevention. Water Resour. Res. 34:505–516.

Mohanty, B.P., J.S. Famiglietti, and T.H. Skaggs. 2000a. Evolution of soil moisture spatial structure in a mixed vegetation pixel during the Southern Great Plains 1997 (SGP97) Hydrology Experiment. Water Resour. Res. 36:3675–3686.

Mohanty, B.P., and T.H. Skaggs. 2001. Spatio-temporal evolution and time-stable characteristics of soil moisture within remote sensing footprints with varying soil, slope, and vegetation. Adv. Water Resour. 24(9–10):1051–1067.

Mohanty, B.P., T.H. Skaggs, and J.S. Famiglietti. 2000b. Analysis and mapping of field-scale soil moisture variability using high-

resolution, ground-based data during the Southern Great Plains 1997 (SGP97) Hydrology Experiment. Water Resour. Res. 36: 1023–1031.
Mohr, K.I., J.S. Famiglietti, A. Boone, and P.J. Starks. 2000. Modeling soil moisture and surface flux variability with an untuned land surface scheme: A case study from the Southern Great Plains 1997 Hydrology Experiment. J. Hydrometeorol. 1(2):154–169.
Mualem, Y. 1976. A new model predicting the hydraulic conductivity of unsaturated porous media. Water Resour. Res. 12:513–522.
Njoku, E.G., and D. Entekhabi. 1995. Passive remote sensing of soil moisture. J. Hydrol. 184:101–130.
Paniconi, C., S. Kleinfeldt, J. Deckmyn, and A. Giacomelli. 1999. Integrating GIS and data visualization tools for distributed hydrologic modeling. Trans. GIS 3:97–118.
Prevot, L., R. Bernard, O. Taconet, D. Vidal-Madjar, and J.L. Thony. 1984. Evaporation from a bare soil evaluated using a soil water transfer model and remotely sensed surface soil moisture data. Water Resour. Res. 20:311–316.
Renschler, C.S. 2003. Designing geo-spatial interfaces to scale process models: The GeoWEPP approach. Hydrol. Processes 17: 1005–1017.
Reichle, R., D. McLaughlin, and D. Entekhabi. 2002. Hydrologic data assimilation with the ensemble Kalman filter. Mon. Weather Rev. 130:103–114.
Schmugge, T.J., P. Gloersen, T. Wilheit, and F. Geiger. 1974. Remote sensing of soil moisture with microwave radiometers. Soil Sci. Soc. Am. Proc. 28:721–724.
Schmugge, T.J., J.M. Meeneely, A. Rango, and R. Neff. 1977. Satellite microwave observations of soil moisture variations. Water Resour. Bull. 13:265–286.
Schmugge, T.J., T.J. Jackson, and H.L. McKim. 1980. Survey of methods for soil moisture determination. Water Resour. Bull. 16: 961–979.
Schreier, H., and S. Brown. 2001. Scaling issues in watershed assessments. Water Policy 3:475–489.
Schlosser, A.C., and P.C.D. Milly. 2000. The potential impact on the soil moisture initialization on the soil moisture predictability and associated climate predictability. GEWEX/BAHC International workshop on soil moisture monitoring, analysis and prediction for hydrometeorological and hydroclimatological applications. Workshop Summary Report. Norman, OK.
Sellers, P.J., M.D. Heiser, F.G. Hall, S.J. Goetz, D.E. Strebel, S.B. Verma, R.L. Desjardins, P.M. Schuepp, and J.I. MacPherson. 1995. Effects of spatial variability in topography, vegetation cover and soil moisture on area-averaged surface fluxes. A case study using FIFE 1989 data. J. Geophys. Res. 100:25607–25629.
Simunek, J., M. Sejna, M.Th. van Genuchten, J. Majercak, V. Novak, and J. Sutor. 1997. The HYDRUS-ET software package for simulating the one-dimensional movement of water, heat and Multiple solutes in a variably saturated media. Version 1.1. U.S Salinity Lab., USDA-ARS, Riverside, CA, Institute of Hydrology Slovak Academy of Sciences, Bratislava, Slovakia.
Smith, M.R., and R.W. Newton. 1983. The prediction of root zone soil moisture with a water balance–microwave emission model. AgRISTARS. SMT3-04425. NASA/GSFC.
Starks, P.J., G.C. Heathman, L.R. Ahuja, and L. Ma. 2003. Use of limited soil property data and modeling to estimate root zone soil water content. J. Hydrol. 272:131–147.
Starr, J.L., and I.C. Paltineanu. 1998. Soil water dynamics using multisensor capacitance probes in nontraffic interrows of corn. Soil Sci. Soc. Am. J. 62:114–122.
Thieken, A.H., A. Lûcke, B. Diekkrûger, and O. Richter. 1999. Scaling input data by GIS for hydrological modeling. Hydrol. Processes 13: 611–630.
van Genuchten, M.Th. 1980. A closed-form equation for predicting the hydraulic conductivity of unsaturated soils. Soil Sci. Soc. Am. J. 44:892–898.
Walker, J.P., G.R. Willgoose, and J.D. Kalma. 2001. One-dimensional soil moisture profile retrieval by assimilation of near-surface observations: A comparison of retrieval algorithms. Adv. Water Resour. 24:631–650.
Wickel, A.J., T.J. Jackson, and E.F. Wood. 2001. Southern Great Plains hydrology experiment. Int. J. Remote Sens. 22:1571–1583.
Zhu, J., and B.P. Mohanty. 2002. Upscaling of hydraulic properties for steady state evaporation and infiltration. Water Resour. Res. 38(9): 1178. doi:10.1029/2001WR000704.
Zhu, J., and B.P. Mohanty. 2003a. Effective hydraulic parameters for steady state vertical flow in heterogeneous soils. Water Resour. Res. 39(8):1227. doi:10.1029/2002WR001831.
Zhu, J., and B.P. Mohanty. 2003b. Upscaling of hydraulic properties of heterogeneous soils. p. 97–117. *In* Y. Pachepsky et al. (ed.) Methods of scaling in soil physics. CRC Press, Boca Raton, FL.